Title

Metabolic flux analysis of the neural cell glycocalyx reveals differential utilization of monosaccharides

Journal

Glycobiology, 30(11)

ISSN

0959-6658

Authors

Wong, Maurice

Xu, Gege

Barboza, Mariana

et al.

Publication Date

2020-10-21

DOI

10.1093/glycob/cwaa038

Peer reviewed

Metabolic flux analysis of the neural cell glycocalyx reveals differential utilization of monosaccharides

Keywords: Glycomics, Mass Spectrometry, Metabolic flux analysis, Neuron, Stable isotope labeling

Supplementary Data Included: Figures S1 – S5

Maurice Wong-1, Gege Xu-1, Mariana Barboza-2, Izumi Maezawa-3, Lee-Way Jin-3, Angela Zivkovic-4, Carlito B. Lebrilla-1

1 - Department of Chemistry, University of California, Davis, Davis, California 95616, USA

2 - Department of Anatomy, Physiology & Cell Biology; Department of Chemistry, University of California, Davis, Davis, California 95616, USA

3 - Department of Pathology and Laboratory Medicine, UC Davis Medical Center, Sacramento, California 95817, USA

4 - Department of Nutrition, University of California, Davis, Davis, California 95616, USA

Maurice Wong (Corresponding Author)
Department of Chemistry
University of California, Davis
Davis, California 95616, USA
E-mail: myuwong@ucdavis.edu
Phone number: +1 530 650 6127

Abstract

Saccharides in our diet are major sources of carbon for the formation of biomass such as proteins, lipids, nucleic acids, and glycans. Among the dietary monosaccharides, glucose occupies a central role in metabolism, but human blood contains regulated levels of other monosaccharides as well. Their influence on metabolism and how they are utilized has not been explored thoroughly. Applying metabolic flux analysis on glycan synthesis can reveal the pathways that supply glycosylation precursors and provide a snapshot of the metabolic state of the cell. In this study we traced the incorporation of six ^{13}C uniformly-labeled monosaccharides in the N-glycans, O-glycans, and glycosphingolipids of both pluripotent and neural NTERA-2 cells. We gathered detailed isotopologue data for hundreds of glycoconjugates using mass spectrometry methods. The contributions of *de novo* synthesis and direct incorporation pathways for glucose, mannose, fructose, galactose, N-acetylglucosamine, and fucose were determined based on their isotope incorporation. Co-feeding studies revealed that fructose incorporation is drastically decreased by the presence of glucose, while mannose and galactose were much less affected. Furthermore, increased sialylation slowed down the turnover of glycans but fucosylation attenuated this effect. Our results demonstrated that exogenous monosaccharide utilization can vary markedly depending on the cell differentiation state and monosaccharide availability, and that the incorporation of carbons can also differ among different glycan structures. We contend that the analysis of metabolic isotope labeling of glycans can yield new insights about cell metabolism.

Introduction

Glycans are metabolic products biologically synthesized through non-templated yet highly regulated processes. Glycan biosynthesis is carried out by a host of glycosyltransferases and glycosidases in the endoplasmic reticulum and the Golgi apparatus. Using just a small set of monosaccharide precursors, these enzymes can produce diverse glycan structures which can be elongated with repeating saccharide units, have multiple branching points, and express glycan epitopes (Varki and Sharon 2009). Cellular precursor monosaccharides can be derived from exogenous carbohydrates, salvaged from degraded glycans, converted from other monosaccharides, or synthesized anew through gluconeogenesis (Freeze and Elbein 2009; Yarema and Bertozzi 2001). Pathways that convert glucose to other glycosylation monosaccharide precursors are present in most cells but may be restricted by other factors. The quantitative contributions of each pathway have not been fully elucidated, although several factors are now known to affect glycosylation including the cellular type and state, nutrient availability, and cell culture conditions (Goochee and Monica 1990; Hossler 2012; Park et al. 2017).

Glucose is intricately involved in several metabolic pathways, including routes for ATP production and those that provide precursors for other biological macromolecules. It is one of the most abundant nutrients in human plasma, maintained at levels of around 5.5 mM in healthy subjects. However, other monosaccharides are also present in blood at lower levels than glucose. Mannose is present at 0.050 – 0.100 mM (Sharma et al. 2014), galactose can vary from about 0.23 - 4.56 mM (Williams et al. 1983), and fructose at 0.005 – 0.300 mM (Laughlin 2014).

Despite their relatively low concentrations, both *in vitro* and *in vivo* experiments using isotopically labeled precursors have shown that specific monosaccharides such as fucose, mannose, and galactose are preferred for glycan biosynthesis. Exogenous mannose at physiological levels can provide up to 50% of mannose in the N-glycans of a human fibroblast cell line (Ichikawa et al. 2014). Up to 10%

of orally administered galactose incorporated directly into human milk oligosaccharides (Rudloff et al. 2006). Although fructose is not expressed on glycans, it still a major dietary sugar. High doses of fructose can be circulated in the bloodstream and be utilized by cells (Jang et al. 2018; Sun and Empie 2012). We have recently reported that the rate of incorporation of exogenous monosaccharides into glycoproteins is both glycan-specific and protein-dependent (Xu et al. 2019b). *In vivo* studies on mice, rats, and chicks have shown that intravenously administered radiolabeled fucose incorporate readily into brain glycoproteins (Popov et al. 1976; Rose and Harding 1984; Zatz and Barondes 1970). Radiolabeled glucose, galactose, and glucosamine were also detected in the glycolipids of juvenile rat brains (Burton et al. 1963). These studies illustrate the importance of glycosylation in brain development, especially for learning and memory. A more complete understanding of the contributions of glycan biosynthetic pathways should entail the utilization of not just glucose, but also other monosaccharides.

To investigate the utilization of exogenous monosaccharides in a neural model, we induced the pluripotent human embryonic carcinoma cell line NTERA-2 to differentiate into glial and neuronal cells, then compared the utilization of various monosaccharides towards glycan synthesis before and after differentiation by comprehensive glycomic analysis. Differentiation causes dynamic changes in cell metabolism. Pluripotent cells are still in a proliferative stage, and their metabolic pathways are geared towards anabolic processes to generate the biomass needed for new cells (Vander Heiden et al. 2009). Thus, more glucose is metabolized through glycolysis to supply the required precursors for macromolecular synthesis. By contrast, differentiated cells further metabolize the glycolytic products through the tricarboxylic acid (TCA) cycle and oxidative phosphorylation to yield more energy per glucose molecule. Metabolic profiling studies have revealed that neurons rely on oxidative metabolism for energy, while astrocytes use glycolysis to release lactate that can be taken up by neurons (Bélanger et al. 2011). How this metabolic shift affects glycan synthesis has not yet been elucidated.

Differentiation can also alter the glycomic landscape on the cell surface, reflecting the evolution in the functions of the cell (Hakomori 1981; Lau et al. 2007). Pluripotency is linked to the increased expression of N-glycan high mannose structures (Hasehira et al. 2012) and globo-type glycosphingolipid (GSL) structures, particularly stage-specific embryonic antigens (SSEA) which are regarded as markers for cell pluripotency (Breimer et al. 2017). When differentiated into neural progenitors, GSL expression is shifted from globo- and lacto- type structures to sialylated gangliosides (Liang et al. 2011). The functional roles of these glycan features are not yet fully understood, although it has been shown that SSEA-3 and -4 are not essential to maintain pluripotency in human embryonic stem cells (Brimble et al. 2007).

In this study, we profiled the changes in glycosylation that accompany neural cellular differentiation. We fed both undifferentiated and differentiated NTERA-2 cells with isotopically labeled monosaccharides and quantified their incorporation into cell surface glycans. The glycoconjugates were analyzed through a mass-spectrometry based method that combines previously described methods (Park et al. 2017; Wong et al. 2018) into a single workflow for N-glycan, O-glycan, and GSL analyses. The unified method is benefited by the sensitivity and mass resolution of a chip-based nanoflow Liquid Chromatography system coupled to a Quadrupole/Time-of-Flight Mass Spectrometer (nanoLC-Chip-Q/ToF MS). A more comprehensive profile of the cell surface glycocalyx can thus be obtained from a single sample source. By analyzing intact glycans we can track the differential incorporation of ^{13}C into individual glycan structures. Detailed quantitative isotopologue profiles were gathered for 112 N-glycan, 45 O-glycan, and 96 GSL compositions. To our knowledge, this is the most comprehensive isotopic labeling analysis of cell-surface glycosylation to date. Through these results we delve into how metabolic pathways and glycan synthesis are affected by the availability of various exogenous sugars. We also investigate the turnover rates of different types of protein- and lipid-bound glycans, and how supplementation of glucose with other monosaccharides affects monosaccharide utilization.

Results

Glycomic characterization of differentiated neural cells

The pluripotent embryonic cell line NTERA-2 was differentiated into neurons and glial cells by exposure to retinoic acid for at least 4 weeks following an established differentiation protocol (Thompson et al. 1984). Differentiation was confirmed by morphological changes in the differentiated cells such as the agglomeration of neuronal cells and neurite outgrowth, as shown in **Supplementary Figure S1**. To remove undifferentiated cells and obtain a purer culture of neural cells, the differentiated neural cells were selectively released and replated with a dilute solution of trypsin. The replated cells were exposed to mitotic inhibitors for at least two weeks to prevent the proliferation of undifferentiated cells.

We purified and analyzed the N-glycans, O-glycans, and GSLs from the membrane fractions of the pluripotent and neural cells. Annotated glycan chromatogram profiles of NTERA-2 cells are shown in **Figure 1**. The N-glycan profile shows a notable decrease of high mannose structures from a relative abundance of 35% to 20% and an increase of sialylated structures from 47% to 58% upon neural differentiation. Multiantennary sialylated complex-type structures constituted the majority of N-glycan structures in differentiated neural cells. The O-glycans comprised of mostly sialylated core 2 O-GalNAc glycans elongated with repeating N-acetyllactosamine units, together with sialylated core 1 glycans. O-Mannose structures were not detected in appreciable quantities, but the low abundances were due to limitations of the method and not necessarily because they were absent from NTERA-2. Globo-type GSLs including Gb3, Gb4, and SSEA-3 and -4 were abundant in undifferentiated cells but were mostly undetected or found in much lower levels in neural cells. Gangliosides with multiple sialylation such as GT1, GD3, GD2, and GD1 also increased in neural cells. The shift in the neural glycomic profile towards a

greater abundance and density of sialic acids is in good agreement with published literature, albeit on other cell lines (Breimer et al. 2017; Park et al. 2015).

Patterns of ^{13}C incorporation

To determine how NTERA-2 cells utilize different monosaccharides for glycan synthesis, we separately fed undifferentiated and differentiated neural cells with 5 mM of [^{13}C-UL] glucose, galactose, mannose, fructose, or N-acetylglucosamine for 72 h prior to harvest. We also tested different conditions with [^{13}C-UL] fucose: 5 mM labeled fucose, 100 µM labeled fucose, and 100 µM labeled fucose with 5 mM regular glucose. The isotopologue profiles for hundreds of N-glycan, O-glycan, and GSL structures were determined with the Agilent Profinder B.08 software, which can also correct for the natural distribution of ^{13}C.

With the introduction of ^{13}C in the form of labeled monosaccharides, the observed *m/z* signals of a target glycan analyte were distributed between the unlabeled molecular ion *M* and labeled molecules with higher *m/z* values corresponding to *M + n,* where *n* is the number of ^{13}C. Because we can only observe the mass-to-charge ratio, the observed mass shift would also depend on the charge state: the shift due to each ^{13}C is equivalent to 1 amu divided by the charge state *z*. For example, when *n* = 6, a mass shift of 3 *m/z* is observed for an ion with *z* = 2.

The isotopologue pattern due to the ^{13}C mass shift depended on the metabolic pathways leading to the incorporation of the monosaccharide. We identified two distinct patterns of incorporation: intact incorporation, which is associated with direct incorporation and salvage pathways; and diffused incorporation, which is associated with glycolytic pathways and *de novo* synthesis of monosaccharides. Intact incorporation of uniformly labeled monosaccharides was distinguished by discrete signals every 6 units after the glycan molecular ion, corresponding to the six labeled carbons in each [^{13}C-UL] monosaccharide. Diffused incorporation was characterized by a broad distribution of *M + n* signals. Both

intact and diffused incorporation patterns are illustrated in **Figure 2**, which shows the isotopologue profiles for representative N-glycan, O-glycan, and GSL compounds chosen for their abundance. The selected compounds illustrate the trends found in their respective types.

The monosaccharides glucose, galactose, mannose, and fructose displayed mostly diffused incorporation in both undifferentiated pluripotent cells and differentiated neural cells, demonstrating that they are broken down through glycolysis before being incorporated back in newly synthesized monosaccharides. Lower levels of intact incorporation were also observed for the four hexoses, but to varying degrees depending on glycan type and differentiation state. It is noteworthy that their isotopologue distribution patterns were vastly dissimilar despite undergoing the same catabolic processes.

In contrast, N-Acetylglucosamine (GlcNAc) and fucose (Fuc) were mostly incorporated intact in NTERA-2 cells. GlcNAc was converted to N-acetylgalactosamine (GalNAc) and N-acetylneuraminic acid (NeuAc) in pluripotent cells. It displayed conversion to only GalNAc and but not NeuAc in neural cells. This effect can be observed in **Figure 2B.** Here, the GlcNAc-treated undifferentiated sample (6^{th} mass spectrum from the top) showed a prominent signal at *M + 30*, corresponding to the intact incorporation of 4 GlcNAc and 1 NeuAc residues in the glycan structure; the same signal was not observed in the neural cell sample, indicating that the conversion pathway of GlcNAc to NeuAc is lost after differentiation. This same pattern was also observed in other sialylated glycans, including O-glycans and GSLs.

Interestingly, fucose showed only direct incorporation without interconversion to other monosaccharides. Fucose incorporation was exceptionally efficient and highly specific. Intact incorporation of fucose remained at the same level even when the concentration was lowered from 5 mM to 100 μM. It was also unaffected by the presence of 5 mM glucose.

Isotopologue quantitation

Unique isotopologue profiles were obtained for each analyzed glycan species. We devised some metrics to summarize the data and compare them more easily. The percentage of labeling (*%L*) is the simplest measure, and can be calculated by taking the difference between 100% and the corrected *M + 0* relative abundance. However, *%L* can only indicate how much of a given glycan has incorporated at least one ^{13}C from exogenous sources; it does not provide a measure of *how many* ^{13}C atoms were incorporated in a specific glycan. Incorporation of more ^{13}C in a glycan would result in a shift towards higher *M + n*, as can be seen from the isotopologue plots in **Figure 2**. The *%L* will also give higher values for glycans with more monosaccharide residues because of the cumulative probability of each monosaccharide being labeled. Thus, it would display an inherent bias towards N-glycans because they typically have more monosaccharide units than O-glycans and GSLs.

A more meaningful measurement of ^{13}C incorporation would account for the shift isotopologue distribution towards higher masses. To make more direct comparisons, we calculated for the percent extent of incorporation (*%E*) as a measure of the completeness of ^{13}C labeling, normalized to the number of carbon atoms of the glycan. The %E was defined by the following equation:

$$\%E = \sum_{n=1}^{N} \frac{n \times (\%\ \text{Corrected Abundance})_n}{N}$$

Where n was the number of ^{13}C in the isotopologue and N was the total number of carbons in the glycan. This allowed us to compare not just glycans of different sizes, but also different kinds of glycoconjugates.

A conservative estimate of the extent of intact incorporation (*%Ei*) was also calculated by considering only the *M + 6n* signals and subtracting the average of the *(M + 6n) ± 1* signals to account for diffused incorporation and normalizing the signal to the number of carbon atoms. We then calculated

for the extent of diffused incorporation (*%Ed*) by subtracting *%Ei* from *%E*. The mean *%E* of N-glycans, O-glycans, and GSLs extracted from undifferentiated and neural cells grown with labeled monosaccharides are shown in **Figure 3A**, while **Figure 3B** shows the mean *%Ei* and *%Ed*.

Here we briefly discuss the sources of error for these measurements. Instrument noise can introduce error because we are taking a summation of signals from a large discontinuous range of *m/z*. This is most noticeable in the incorporation values from control samples. Noise will disproportionately affect low abundance compounds and larger compounds, which will require a larger *m/z* range. We mitigated this issue by discarding compounds with an area count lower than 100,000 and setting the mass tolerance at 10 PPM during peak extraction. We also screened out co-eluting compounds with overlapping *m/z* ranges to avoid erroneous readings. Another source of error was the small amount of impurity in the uniformly labeled monosaccharides (99% purity according to manufacturer's analysis). This includes partially labeled monosaccharides, which would lead to the underestimation of intact incorporation, *%Ei*, and concomitantly an overestimation of *%Ed*. In glycans with particularly high levels of intact incorporation in a high number of monosaccharide residues, the signals from partially labeled monosaccharides add up and compromise our calculations for *%Ei*. This effect was observed in high-mannose N-glycans, but it was not as pronounced in most other structures. We also saw this in the *%Ed* values from samples with labeled fucose although they are only incorporated intact. Despite these caveats, the calculated *%E* values still provide a convenient summary of the data.

Nature of isotopic incorporation in pluripotent and neural cells

Undifferentiated pluripotent cells rely more heavily on glycolytic pathways to metabolize glucose and other monosaccharides into anabolic precursors. Activated monosaccharides can also be utilized directly for glycan synthesis; indeed, this would be more energetically efficient. We calculated the contributions from these pathways from the glycan isotopologue profiles of pluripotent and neural

cells fed for 72 h with labeled monosaccharides. The carbon contributions from exogenous monosaccharides exhibited a wide range among the different glycan structures, from just a few percent to about 70% in the largest high mannose N-glycans of fructose-fed pluripotent cells. To compare the different conditions, we plotted the mean *%E* values in **Figure 3**. Here we note that a considerable amount of carbons was not sourced from exogenous monosaccharides. Exogenous glucose provided an average of just 16% of the carbons in all three glycoconjugate types in pluripotent cells. This figure was at around 26 – 27% in protein-bound glycans and 11% in GSLs after differentiation. We surmise that the unlabeled carbons could be derived from the 4 mM glutamine in the growth media. Among the monosaccharide-derived carbons, we observed predominantly diffused incorporation patterns from exogenous glucose, galactose, mannose, and fructose, suggesting that the monosaccharide precursors for glycan synthesis were heavily sourced from the gluconeogenesis of glycolytic products rather than intact incorporation of activated monosaccharides. This effect was most pronounced when mannose and fructose were provided to pluripotent cells, in which they contributed a mean *%Ed* of 39% and 57% respectively to N-glycans; these figures are 2.6 and 3.8 times greater than that of glucose. Mannose and fructose incorporation exhibited the most distinct differences between pluripotent and neural cells. The mean *%Ed* of glucose and galactose both pre- and post-differentiation stood at 15 – 17% in N- and O-glycans.

By contrast, intact incorporation of the four hexoses contributed just between 2 – 8% in all glycoconjugates. In both pluripotent and neural cells, galactose found a modestly higher level of intact incorporation in O-glycans and GSLs, in which its *%Ei* stood at 6.7 – 8.7% compared to around 2% in N-glycans. This was due to the prevalence of Gal and GalNAc in these structures. The utilization of galactose is regulated by the Leloir pathway (Frey 1996), which converts galactose to glucose; this limits the conversion of galactose to other monosaccharides and its access to glycolytic pathways.

Delving into the *%E* of individual glycan structures in **Supplementary Figure S2** reveals some glycan specificity of intact incorporation. Among GSLs in pluripotent cells, the *%Ei* of galactose is highest in globo-type GSLs, particularly in Gb3, SSEA-3, and SSEA-4 (labeled as *3_0_0_0_0_0_d34_1*, *4_1_0_0_0_0_d34_1*, and *4_1_0_1_0_0_d34_1* respectively). The values were comparable only to lactosylceramides, which are the common precursors for all GSLs (glycan composition of *2_0_0_0_0_0*). This indicates a fast rate of synthesis for globo structures since glycolytic steps are avoided.

Mannose was incorporated intact most rapidly in high-mannose N-glycans, which were especially abundant in pluripotent cells. This partially accounted the higher overall *%E* of mannose in pluripotent cells. Incorporation of mannose in N-glycans was notably decreased in neural cells, and a bigger share was taken up by O-glycans. Exogenous mannose was shunted heavily towards N-glycosylation pathways during the proliferative state.

Fructose presented the highest level of diffused incorporation among all the monosaccharides. Its phosphorylated form can readily enter the glycolysis pathway, and its high *%Ed* implied an increased rate of glycolysis and gluconeogenesis in pluripotent cells. This was attenuated after neural differentiation. From **Supplementary Figure S2**, we also observe an *%Ei* of around 10 – 20% (pluripotent) and 5 – 11% (neural) in high mannose N-glycans, indicating that fructose was converted to mannose as well.

The *%E* in GSLs was generally higher in pluripotent cells than in neural cells, demonstrating a faster rate of GSL synthesis in the proliferative pluripotent cells. In GSLs, glucose and fructose also shifted from diffused to intact incorporation after neural differentiation, as seen in **Figure 2D**. The incorporation of galactose and mannose in GSLs remained mostly intact. Glycolytic products from glucose and fructose might also be utilized for lipid synthesis in GSLs as seen in their diffused incorporation patterns, although the contribution from this pathway seemed to be low. It is also notable

that the contribution of glycolytic pathways to GSLs after differentiation was more moderate compared to N-glycans and O-glycans, although intact incorporation remained at similar levels.

Fucose (Fuc) exhibited only intact incorporation and showed no glycolytic contributions towards glycan synthesis even in the absence of glucose. N-Acetylglucosamine (GlcNAc) had only very low levels of diffused incorporation without glucose. Note that the small value of *%Ed* in the fucose data presented in **Figure 3B** was due to signal noise and the underestimation of intact incorporation as described in the previous section. The *%Ei* of GlcNAc in N- and O-glycans was relatively higher at 12 – 13% in pluripotent cells because of its conversion to GalNAc and NeuAc. However, conversion of GlcNAc to NeuAc was massively reduced post-differentiation, despite the heavy sialylation of the neural glycome. This effect suggested a loss of UDP-GlcNAc 2-epimerase activity (Keppler et al. 1999) and perhaps an efficient salvage pathway for sialic acids. The specificity of fucose incorporation remained unchanged although lower levels were found after differentiation. The observed monosaccharide interconversions were in line with known pathways and further highlight the unique routes taken by fucose and GlcNAc towards incorporation.

Co-feeding studies demonstrate the effect of glucose levels on monosaccharide utilization

Co-feeding studies were performed to better simulate the extracellular environment in mammals, where the supply of glucose is well-regulated by complex biological systems (Cura and Carruthers 2011). Human blood glucose levels are maintained at 5.5 mM in healthy individuals, and deviations induce rapid homeostatic responses to restore normal levels. To test how cells utilize other monosaccharides under hypoglycemic conditions, pluripotent cells were provided with 0, 0.10 mM, 0.25 mM, 0.50 mM, 1 mM, or 5 mM of normal glucose together with 5 mM of either [^{13}C-UL] galactose, mannose, or fructose for 24 h. The N-glycan isotopologue data are summarized in **Figure 4A**, and representative isotopologue profiles from one of the more abundant glycans, Hex5HexNAc4Fuc1NeuAc1,

are shown in **Figure 4B**. The *%Ei* and *%Ed* of individual glycan compositions are plotted in **Supplementary Figure S3.**

The effect of exogenous glucose on the utilization of galactose, mannose, and fructose in N-glycans differed markedly. At exogenous glucose levels of 0 – 1 mM, galactose had a relatively low diffused incorporation at 3.8 – 5.3% and it was mostly incorporated intact, with a mean *%Ei* of 3.7. Galactose was also observed to be converted to other hexoses, as illustrated by the signals at *M + 18* and *M + 24* in the first 5 isotopologue plots in the first column of **Figure 4B**. These signals are lost in the bottommost plot. The high *%Ei* : *%Ed* ratio was consistent with the Leloir pathway, which converts galactose to UDP-galactose and UDP-glucose (Frey 1996).

At 5 mM glucose, the conversion of galactose was minimized and was mostly directly incorporated; the same effect was observed in all glycans. The utilization of mannose remained largely unaffected even at 5 mM Glc, with an *%Ed* of around 25% and an %Ei of 6.0 – 7.8%. Mannose also displayed interconversion at all glucose levels, showing that its utilization was relatively insensitive to the presence of glucose.

On the other hand, the *%Ed* of fructose decreased with increasing glucose concentration. The *%Ed* and *%Ei* of fructose at low glucose concentrations were at around 20% and 8% respectively, comparable to mannose. At 5 mM glucose, the overall incorporation of fructose was vastly minimized to less than 3%. Fructose utilization showed the most sensitivity to glucose supplementation.

The uniformity of the *%Ei* : *%Ed* ratio for the mannose-glucose and fructose-glucose combinations suggested that the initial action of hexokinase was the limiting factor, rather than the epimerases/isomerases that convert mannose-6-phosphate and glucose-6-phosphate to fructose-6-phosphate (Freeze and Elbein 2009). These results implied that the hexokinase had a stronger preference for mannose over glucose, and the least for fructose.

Time-course studies yield differential incorporation in glycan types

Time-course experiments further revealed the rates of synthesis and glycan turnover. In this study, the concentration of labeled glucose was matched to the level in the DMEM growth medium at 25 mM. Although this is higher than the physiological level of 5 mM, it allowed for a higher level of ^{13}C incorporation within the 24 h timeframe and better quantitation of isotopologues. Undifferentiated cells were provided with 25 mM [^{13}C-UL] glucose for 3, 6, 9, 12, 18, and 24 h prior to harvest. The rates of synthesis of new glycans can be observed within this 24 h timeframe. **Figure 5** illustrates the mean *%Ei* and *%Ed* for N- and O-glycans as well as GSLs. The incorporation shifted towards a higher *M + n* over time and towards higher abundance of labeled isotopologues, leading to an increase in *%E*. The increase of diffused incorporation was much faster than that of intact incorporation. The *%Ed* in N-glycans continued to increase for 24 h at a rate of 1.8% per hour, while it plateaued at 18 h in O-glycans and GSLs at rates of 1.4% per hour and 0.9% per hour respectively. The *%Ei* increased at a rate of only 0.2%, 0.4%, and 0.3% per hour for N-glycans, O-glycans, and GSLs respectively, although we must note that the *%Ei* was underestimated especially for high-mannose structures.

Differential incorporation rates were observed among different subtypes. Glycans with the highest rates also displayed the most intact incorporation, and these were mostly the precursors of each type: high-mannose structures in N-glycans, and the GSL precursors monohexosylceramide and lactosylceramide. Globo-type GSLs also displayed higher levels of intact incorporation than gangliosides, as shown in **Supplementary Figure S4**.

In N-glycans, the rates of incorporation followed the maturity of N-glycans. As shown in **Figure 6B,** incorporation was fastest in high-mannose structures, followed by hybrid and then complex structures as expected from the N-glycan biosynthetic pathway (Kornfeld and Kornfeld 1985; Stanley et

al. 2015). The incorporation curve of complex- and hybrid- type N-glycans (**Figure 6B**) was similar to that of the paucimannose structure $GlcNAc_2Man_3$ (**Figure 6A**), suggesting that the trimming of mannoses through the successive activity of mannosidases determined the rate of N-glycan formation.

Hybrid- and complex-type N-glycans reached mean *%E* of 50% and 40% respectively after 24 h. Higher antennarity in complex-type N-glycans led to slower incorporation as expected from the N-glycan biosynthetic pathway. Increased sialylation led to slower turnover rates, and this effect was most apparent in tri-antennary N-glycans; however, core fucosylation modulated this behavior, as shown in **Figure 6C**. The trend was also observed among bi-antennary N-glycans as well as sialylated O-glycans. These results suggest that sialylation and core fucosylation both play a role in glycoprotein turnover. The decreasing effect of sialylation on glycan turnover was also observed in previous work on a hepatic cholangiocarcinoma cell line M213 (Xu et al. 2019a).

In GSLs, the main determinant of incorporation rate was the length of the ceramide N-linked fatty acid, as shown in **Figure 6D**. For GSLs with the same glycan headgroups, a shorter lipid length led to higher incorporation and therefore faster turnover compared to those with a longer fatty acid chain, consistent with the results reported by Skotland et al. (Skotland et al. 2016).

Reproducibility

To estimate the reproducibility of the experiment, 2 biological replicates were performed for the provision of 5 mM [^{13}C-UL] glucose, mannose, and fructose to undifferentiated NTERA-2 for 24 h. Triplicates were performed for labeled galactose. Unfortunately, replicates could not be accomplished for all the conditions in the experiment due to the cost of isotopically labeled reagents. Biological replicates were grown from the same passage of cells. In general, the glycomic profiles were similar among replicates. The ^{13}C incorporation patterns and relative quantities were also largely similar among the replicates. The calculated *%E* for each N-glycan composition are plotted in **Supplementary Figure S5**,

with error bars representing the standard deviation (SD). Compounds with higher abundances and higher levels of incorporation had lower standard deviations. An average of around 5% SD was calculated for the *%E* among the different glycans in biological duplicates, showing that the incorporation of ^{13}C and isotopologue quantitation method presented are reproducible.

Discussion

Akin to metabolic flux analysis, studying how exogenous monosaccharide precursors are incorporated into glycans can reveal the pathways taken by the monosaccharides and provide a snapshot of the metabolic state of the cell. Most of the metabolic analyses reported using ^{13}C stable isotope labeling have focused on small molecule metabolites such as amino acids or phosphorylated monosaccharides (Dalman et al. 2016; Ichikawa et al. 2014; Zamboni et al. 2009). The application of stable isotope tracers to macromolecules such as oligosaccharides and glycolipids presented new challenges. First, a broader range of *m/z* values must be monitored corresponding to the number of carbons in the analyte, leading to a greater chance of isotopologue signal overlap. Second, the distribution of the target analyte among multiple isotopologues could diminish signal intensity by an order of magnitude or more. These challenges can be addressed by good chromatographic separation and sensitive detection. Nanoflow LC-MS using a chip-based enrichment and analytical column coupled to a time-of-flight (TOF) MS has proven to be up to the task and was the implement of choice for this study. Finally, the deconvolution of the natural isotopic distribution of a large biomolecule was necessary to tease out the contributions of exogenous isotope labeling. Valkenborg and others offer an excellent review of modern computational methods to address this problem (Valkenborg et al. 2012). The Agilent Profinder B.08 software provided the much-needed algorithm for this deconvolution.

We observed two patterns in the corrected/deconvoluted isotopologue profiles. The sharp and distinct mass shifts corresponding to 6 carbons were easily discernible as the intact incorporation of

monosaccharides. The broad distributions, which we described as diffused incorporation, signaled that the glycan analyte contained a mix of monosaccharide residues with different numbers of labeled carbons. The monosaccharide residues were synthesized not just from glycolytic pyruvate, which would result in uniform mass shifts of 3 units. The gluconeogenesis pathway could also take its precursors from the intermediates in the TCA cycle or the breakdown of recycled amino acids which have incorporated the labeled carbons, resulting in hexoses with 2, 3, 4, or 5 labeled carbons. By taking the summation of these corrected isotopologue signals, we were able quantify the amount of glycolytic metabolites that feed into the gluconeogenesis pathway (Exton 1972).

The provision of 5 mM labeled glucose for 72 h yielded only an average of 16% incorporation in the protein-bound glycans of pluripotent cells and up to 27% in neural cells, showing that other carbon sources such as glutamine in the growth medium can also contribute heavily to glycan synthesis. In both differentiation states, the contribution from the intact incorporation of exogenous glucose was notably much lower than from diffused incorporation; the same was true for galactose, mannose, and fructose when supplied without glucose. These monosaccharides were effectively shunted to glycolytic pathways in both pluripotent and neural NTERA-2 cells, with relatively smaller amounts left for glycan synthesis. Our results further demonstrated that the neural NTERA-2 still retained much of the metabolic machinery of its undifferentiated pluripotent state despite the vestiges of neural morphology and glycome.

We are likely observing the byproducts of the Warburg effect, the phenomenon by which cells perform enhanced glycolysis even in aerobic conditions (Warburg 1956). It has been postulated that this is mainly for the provision of carbons to generate biomass (Lunt and Vander Heiden 2011). Human embryonic stem cells and induced pluripotent stem cells also exhibit increased glycolysis similar to the Warburg effect (Varum et al. 2011). Nevertheless, the circuitous path of monosaccharide degradation

and *de novo* synthesis was a surprising result because gluconeogenesis is a costly process in terms of energy, and its regulation is reciprocal to glycolysis.

The isotopologue distributions offered some clues to this seeming contradiction. Diffused incorporation patterns occur when monosaccharides utilized for glycan synthesis source their carbons from the intermediates of the TCA cycle or their products. In intact GSLs, minimal glycolytic flux to the lipid portion was observed. We posit that the glycolytic flux went mostly towards amino acid synthesis. The time-course results showed that precursor glycan structures such as N-glycan high-mannose glycans used mostly intact monosaccharides even after 24 h, but the proportion of diffused incorporation was higher for those with slower incorporation rates such as complex N-glycans. In other words, exogenous monosaccharides were more likely to be incorporated intact in less mature glycans, which are usually built up in the endoplasmic reticulum. Taken together, these results suggested that there could be separate sublocalization of monosaccharides from exogenous sources and from gluconeogenesis that feed into different pools. The possibility of having multiple pools of monosaccharide derivatives from different sources has been suggested previously (Ichikawa et al. 2014).

It is important to note that the differentiated NTERA-2 cultures contained a mix of glial and neuronal cells, and the monosaccharide utilization of each cell type cannot be distinguished. Further studies are needed to elucidate the metabolic crosstalk and codependence between glial and neuronal cells.

In this work, we studied the changing glycome of pluripotent NTERA-2 cells undergoing neural differentiation through mass-spectrometry based glycan analysis. We also traced the contributions of glycolytic and direct incorporation pathways towards glycan synthesis by integrating stable isotope labeling into the analytical platform. The ^{13}C incorporation profiles of both pluripotent and neural cells indicated a Warburg-like metabolic state. The results further suggest that sialylation and core

fucosylation could affect glycoprotein turnover. The analytical workflow for the stable isotope labeling of glycans provides another piece of the puzzle in the fluxomic analysis of the whole cell. In future studies, the assay can be further applied towards studying the effect of various stimuli on carbohydrate utilization and other related systems.

Methods

Cell culture. Human pluripotent testicular embryonal carcinoma NTERA-2 cells (RRID: CVCL_3407) were obtained from American Type Culture Collection and cultured in Dulbecco's Modified Eagle's Medium (DMEM), supplemented with 10% (v/v) fetal bovine serum (Gibco), and 100 U/ml penicillin and 100 μg/ml streptomycin (Gibco). Cells were grown in 100 mm cell culture dish. The medium was replaced every 2-3 days, and cells were subcultured on reaching around 80% confluence using 0.05% trypsin (Gibco). Cells were grown in at 37 °C in a humidified incubator with 5% CO_2.

^{13}C-labeled monosaccharide feeding. For a set number of hours prior to harvest, the growth media is changed to a glucose-free formulation of DMEM supplemented with the appropriate [^{13}C-UL] monosaccharide (Omicron Biochemicals) or a combination of uniformly labeled and naturally labeled monosaccharides. The growth medium was supplemented with penicillin and streptomycin, but not fetal bovine serum to avoid the presence of other exogenous monosaccharides. For the hexoses glucose, galactose, mannose, and fructose, a concentration of 5mM was chosen so that a comparison can be made at the physiological level of glucose. Undifferentiated cells were given labeled monosaccharides at approximately 80% confluence and were collected at 100% confluence. It should be noted that the [^{13}C-UL] monosaccharides have a of 99% and would contain some incompletely labeled compounds that can ultimately lower the extent of incorporation.

Neural differentiation. We followed a procedure adapted from Pleasure (Pleasure et al. 1992). Neural differentiation was induced in NTERA-2 cells by supplementing the growth medium with 0.01

mM trans-retinoic acid for at least 4 weeks. Neuronal and glial NTERA-2 cells were selectively detached and replated by using 0.025% trypsin and delivering ten hard taps to both sides of the T75 culture flask. Replated cells were maintained with growth medium supplemented with the following mitotic inhibitors: 1 μM cytosine arabinoside, 10 μM fluoro-deoxyuridine, and 10 μM uridine. Differentiated cells were maintained with mitotic inhibitors for at least 2 weeks before the introduction of labeled monosaccharides.

Membrane extraction. Harvested cells were suspended in homogenization buffer containing 1:100 protease inhibitor cocktail set V (Calbiochem), 0.25 M sucrose, and 20 mM HEPES, with the pH adjusted to 7.5 using KOH. The cells were lysed with a probe sonicator. Nuclear fractions were pelleted and discarded through centrifugation at 2,000 × g for 10 min. Membrane fractions were then pelleted and separated from other subcellular components through a series of ultracentrifugation steps at 200,000 × g for 45 min. This approach has previously been shown to yield a pure membrane fraction based on SDS-PAGE gel electrophoresis and Western blotting using organelle-specific antibodies (An et al. 2012); the contributions from ER and Golgi membranes were shown to be minimal.

Unified N-glycan, O-glycan, and glycolipid extraction. Pelleted membrane fractions were resuspended in 100 μl of 5 mM dithiothreitol in 100 mM phosphate buffer adjusted to a pH of 7. Proteins were denatured by heating at 100°C for 1 min. N-glycans were released enzymatically by digesting with 2 μl of peptide N-glycosidase F (New England Biolabs) at 37°C for 18 h. Samples were then ultracentrifuged at 200,000 g for 45 min. From the supernatant, N-glycans were purified through porous graphitized carbon (PGC) solid phase extraction (SPE). The pellet was washed with 500 μl of a mixture of 3:8:4 (v/v/v) water/methanol/chloroform Folch solvent (Folch et al. 1957) and centrifuged to separate the pelletized proteins from the dissolved lipids in the supernatant. To the supernatant, 100 μl of 0.1 M potassium chloride was added to cause phase separation between the water- and methanol-

rich upper layer, which contains mostly GSLs, and the chloroform-rich lower layer, which contains mostly other lipids such as cholesterol and phospholipids. The upper Folch layer was collected, and GSLs were purified using C8 SPE. O-glycans were released from the pelletized proteins through beta elimination reaction using 200 μl of 0.1 M NaOH and 1 M $NaBH_4$ for 18 h. The reaction was quenched by adding 115 μl of 10% acetic acid. O-glycans were purified by PGC SPE followed by hydrophilic interaction liquid chromatography (HILIC) SPE.

NanoHPLC Chip-Q-TOF MS analysis. All samples were analyzed with an Agilent 6520 Accurate Mass Q-TOF LC/MS equipped with a microfluidic chip, which incorporates an enrichment column, an analytical column, and a nanoelectrospray tip in a single assembly. Purified N-glycan and O-glycan samples were separately reconstituted in 30 μl water and analyzed with a PGC chip. The binary gradient consisted of (A1) 0.1% formic acid and 3% acetonitrile in water, and (B1) 1% formic acid and 89% acetonitrile in water. The LC was programmed to hold the solvent composition at 100% A1 from 0-2.5 min, linearly ramp to 16% B1 at 20 min, and further increase B1 to 58% at 35 min at a constant flow rate of 0.3 μl/min. For isotopologue data acquisition, the Q-TOF MS was set to acquire only MS^1 in positive ionization mode with a cycle time of 1.5 s. To assist with compound identification, control samples were also run with collision-induced dissociation (CID) using nitrogen gas. Four MS^2 spectra were obtained for every MS^1 through data-dependent acquisition, with a total cycle time of 5.25 s. The mass range was set at 600-2000 *m/z* for N-glycan analysis, and at 300-2000 *m/z* for O-glycan analysis. The instrument was calibrated with the ESI tuning mix commercially available from Agilent.

Purified intact GSL samples were reconstituted in 50 μl 1:1 methanol/water and analyzed with a C18 microfluidic chip. A binary gradient consisting of (A2) 20 mM ammonium acetate and 0.1% acetic acid in water, and (B2) 20 mM ammonium acetate and 0.1% acetic acid in 85:15 (v/v) methanol/isopropanol was used to separate the GSLs at a flow rate of 0.3 μl/min. The acquisition method was programmed to increase the percentage of B2 from 70% to 85% over 4 min, then to 100%

at 40 min. The Q-TOF MS was programmed with the same parameters as stated above. The mass range was set at 600-2000 *m/z* for GSL analysis. In all acquisition methods, the columns were flushed with 100% of solvent B for 10 min and equilibrated with the initial solvent composition for another 10 min prior to sample injection.

Data processing and isotopologue analysis. We used Agilent MassHunter B.07 software for initial data processing and compound peak identification. In brief, compound peaks are extracted by matching MS signals with theoretical monoisotopic masses of glycans to within 10 ppm mass tolerance. The assignments are further confirmed by MS2 fragmentation when available. From the exported data, we then create a new library containing the chemical formulae and retention times of identified glycoconjugates for targeted isotopologue extraction. The Agilent Profinder B.08 software was used to extract quantitative isotopologue data for each identified glycan through its Batch Isotopologue Analysis function. The program averages the MS signals across a chosen peak in an extracted ion chromatogram to form the MS spectra from which isotopologue signals are extracted. It also corrects for the natural distribution of ^{13}C and returns the relative abundance of each isotopologue. Mass tolerance was set at ± (10 ppm + 2 mDa) to screen out background noise or signals from other co-eluting compounds. For each glycan, the percent abundance of each isotopologue signal from *M + 0* to *M + n*, where n is the total number of carbons in the glycan, can then be exported for further analysis.

Funding

This work was supported by the National Institutes of Health [grant numbers R01GM049077, R01AG062240].

Declaration of Interests

The authors declare no competing interests.

References

An HJ, Gip P, Kim J, Wu S, Park KW, McVaugh CT, Schaffer DV, Bertozzi CR, Lebrilla CB. 2012. Extensive determination of glycan heterogeneity reveals an unusual abundance of high mannose glycans in enriched plasma membranes of human embryonic stem cells. Molecular & Cellular Proteomics. 11(4):M111.010660.

Bélanger M, Allaman I, Magistretti Pierre J. 2011. Brain energy metabolism: Focus on astrocyte-neuron metabolic cooperation. Cell Metabolism. 14(6):724-738.

Breimer ME, Säljö K, Barone A, Teneberg S. 2017. Glycosphingolipids of human embryonic stem cells. Glycoconjugate journal. 34(6):713-723.

Brimble SN, Sherrer ES, Uhl EW, Wang E, Kelly S, Merrill AH, Robins AJ, Schulz TC. 2007. The cell surface glycosphingolipids ssea-3 and ssea-4 are not essential for human esc pluripotency. STEM CELLS. 25(1):54-62.

Burton RM, Garcia-Bunuel L, Golden M, Balfour YM. 1963. Incorporation of radioactivity of d-glucosamine-1-c14, d-glucose-1-c14, d-galactose-1-c14, and dl-serine-3-c14 into rat brain glycolipids*. Biochemistry. 2(3):580-585.

Ceroni A, Maass K, Geyer H, Geyer R, Dell A, Haslam SM. 2008. Glycoworkbench: A tool for the computer-assisted annotation of mass spectra of glycans. Journal of Proteome Research. 7(4):1650-1659.

Cura AJ, Carruthers A. 2011. Role of monosaccharide transport proteins in carbohydrate assimilation, distribution, metabolism, and homeostasis. Comprehensive Physiology. 2(2):863-914.

Dalman T, Wiechert W, Nöh K. 2016. A scientific workflow framework for 13c metabolic flux analysis. Journal of Biotechnology. 232:12-24.

Exton JH. 1972. Gluconeogenesis. Metabolism. 21(10):945-990.

Folch J, Lees M, Sloane-Stanley G. 1957. A simple method for the isolation and purification of total lipids from animal tissues. The Journal of biological chemistry. 226(1):497-509.

Freeze HH, Elbein AD. 2009. Glycosylation precursors. Essentials of glycobiology 2nd edition. Cold Spring Harbor Laboratory Press.

Frey PA. 1996. The leloir pathway: A mechanistic imperative for three enzymes to change the stereochemical configuration of a single carbon in galactose. The FASEB Journal. 10(4):461-470.

Goochee CF, Monica T. 1990. Environmental effects on protein glycosylation. Bio/Technology. 8(5):421-427.

Hakomori S-i. 1981. Glycosphingolipids in cellular interaction, differentiation, and oncogenesis. Annual review of biochemistry. 50(1):733-764.

Hasehira K, Tateno H, Onuma Y, Ito Y, Asashima M, Hirabayashi J. 2012. Structural and quantitative evidence for dynamic glycome shift on production of induced pluripotent stem cells. Molecular & Cellular Proteomics. 11(12):1913-1923.

Hossler P. 2012. Protein glycosylation control in mammalian cell culture: Past precedents and contemporary prospects. In: Hu WS, Zeng A-P, editors. Genomics and systems biology of mammalian cell culture. Berlin, Heidelberg: Springer Berlin Heidelberg. p. 187-219.

Ichikawa M, Scott DA, Losfeld M-E, Freeze HH. 2014. The metabolic origins of mannose in glycoproteins. Journal of Biological Chemistry. 289(10):6751-6761.

Jang C, Hui S, Lu W, Cowan AJ, Morscher RJ, Lee G, Liu W, Tesz GJ, Birnbaum MJ, Rabinowitz JD. 2018. The small intestine converts dietary fructose into glucose and organic acids. Cell metabolism. 27(2):351-361.e353.

Keppler OT, Hinderlich S, Langner J, Schwartz-Albiez R, Reutter W, Pawlita M. 1999. Udp-glcnac 2-epimerase: A regulator of cell surface sialylation. Science. 284(5418):1372-1376.

Kornfeld R, Kornfeld S. 1985. Assembly of asparagine-linked oligosaccharides. Annual review of biochemistry. 54(1):631-664.

Lau KS, Partridge EA, Grigorian A, Silvescu CI, Reinhold VN, Demetriou M, Dennis JW. 2007. Complex n-glycan number and degree of branching cooperate to regulate cell proliferation and differentiation. Cell. 129(1):123-134.

Laughlin MR. 2014. Normal roles for dietary fructose in carbohydrate metabolism. Nutrients. 6(8):3117-3129.

Liang Y-J, Yang B-C, Chen J-M, Lin Y-H, Huang C-L, Cheng Y-Y, Hsu C-Y, Khoo K-H, Shen C-N, Yu J. 2011. Changes in glycosphingolipid composition during differentiation of human embryonic stem cells to ectodermal or endodermal lineages. STEM CELLS. 29(12):1995-2004.

Lunt SY, Vander Heiden MG. 2011. Aerobic glycolysis: Meeting the metabolic requirements of cell proliferation. Annual Review of Cell and Developmental Biology. 27(1):441-464.

Park D, Brune KA, Mitra A, Marusina AI, Maverakis E, Lebrilla CB. 2015. Characteristic changes in cell surface glycosylation accompany intestinal epithelial cell (iec) differentiation: High mannose structures dominate the cell surface glycome of undifferentiated enterocytes. Molecular & cellular proteomics : MCP. 14(11):2910-2921.

Park D, Xu G, Wong M, Lebrilla CB, Barboza M, Raybould H, Mills DA, Shah IM. 2017. Enterocyte glycosylation is responsive to changes in extracellular conditions: Implications for membrane functions. Glycobiology. 27(9):847-860.

Pleasure S, Page C, Lee V. 1992. Pure, postmitotic, polarized human neurons derived from ntera 2 cells provide a system for expressing exogenous proteins in terminally differentiated neurons. The Journal of Neuroscience. 12(5):1802-1815.

Popov N, Rüthrich HL, Pohle W, Schulzeck S, Matthies H. 1976. Increased fucose incorporation into rat hippocampus during learning. A biochemical and microautoradiographic study. Brain Research. 101(2):295-304.

Rose SPR, Harding S. 1984. Training increases [3h]fucose incorporation in chick brain only if followed by memory storage. Neuroscience. 12(2):663-667.

Rudloff S, Obermeier S, Borsch C, Pohlentz G, Hartmann R, Brösicke H, Lentze MJ, Kunz C. 2006. Incorporation of orally applied 13c-galactose into milk lactose and oligosaccharides. Glycobiology. 16(6):477-487.

Sharma V, Ichikawa M, Freeze HH. 2014. Mannose metabolism: More than meets the eye. Biochemical and Biophysical Research Communications. 453(2):220-228.

Skotland T, Ekroos K, Kavaliauskiene S, Bergan J, Kauhanen D, Lintonen T, Sandvig K. 2016. Determining the turnover of glycosphingolipid species by stable-isotope tracer lipidomics. Journal of Molecular Biology. 428(24, Part A):4856-4866.

Stanley P, Taniguchi N, Aebi M. 2015. N-glycans. In: rd, Varki A, Cummings RD, Esko JD, Stanley P, Hart GW, Aebi M, Darvill AG, Kinoshita T, Packer NH et al., editors. Essentials of glycobiology. Cold Spring Harbor (NY): Cold Spring Harbor Laboratory Press. p. 99-111.

Sun SZ, Empie MW. 2012. Fructose metabolism in humans - what isotopic tracer studies tell us. Nutr Metab (Lond). 9(1):89-89.

Thompson S, Stern PL, Webb M, Walsh FS, Engstrom W, Evans EP, Shi WK, Hopkins B, Graham CF. 1984. Cloned human teratoma cells differentiate into neuron-like cells and other cell types in retinoic acid. Journal of Cell Science. 72(1):37-64.

Valkenborg D, Mertens I, Lemière F, Witters E, Burzykowski T. 2012. The isotopic distribution conundrum. Mass Spectrometry Reviews. 31(1):96-109.
Vander Heiden MG, Cantley LC, Thompson CB. 2009. Understanding the warburg effect: The metabolic requirements of cell proliferation. Science. 324(5930):1029-1033.
Varki A, Cummings RD, Aebi M, Packer NH, Seeberger PH, Esko JD, Stanley P, Hart G, Darvill A, Kinoshita T et al. 2015. Symbol nomenclature for graphical representations of glycans. Glycobiology. 25(12):1323-1324.
Varki A, Sharon N. 2009. Historical background and overview. Essentials of glycobiology 2nd edition. Cold Spring Harbor Laboratory Press.
Varum S, Rodrigues AS, Moura MB, Momcilovic O, Easley CAIV, Ramalho-Santos J, Van Houten B, Schatten G. 2011. Energy metabolism in human pluripotent stem cells and their differentiated counterparts. PLOS ONE. 6(6):e20914.
Warburg O. 1956. On the origin of cancer cells. Science. 123(3191):309-314.
Williams CA, Phillips T, Macdonald I. 1983. The influence of glucose on serum galactose levels in man. Metabolism. 32(3):250-256.
Wong M, Xu G, Park D, Barboza M, Lebrilla CB. 2018. Intact glycosphingolipidomic analysis of the cell membrane during differentiation yields extensive glycan and lipid changes. Scientific Reports. 8(1):10993.
Xu G, Wong M, Li Q, Park D, Cheng Z, Lebrilla CB. 2019a. Unveiling the metabolic fate of monosaccharides in cell membranes with glycomic and glycoproteomic analyses. Chemical Science.
Xu G, Wong M, Li Q, Park DD, Cheng Z, Lebrilla CB. 2019b. Unveiling the metabolic fate of monosaccharides in cell membranes with glycomic and glycoproteomic analyses. Chemical Science.
Yarema KJ, Bertozzi CR. 2001. Characterizing glycosylation pathways. Genome Biology. 2(5):reviews0004.0001.
Zamboni N, Fendt S-M, Rühl M, Sauer U. 2009. 13c-based metabolic flux analysis. Nature Protocols. 4:878.
Zatz M, Barondes SH. 1970. Fucose incorporation into glycoproteins of mouse brain. Journal of Neurochemistry. 17(2):157-163.

Legends to Figures

Figure 1: Extracted compound chromatograms of NTERA-2, showing (A) N-glycan, (B) O-glycan, and (C) GSL profiles of (1) undifferentiated and (2) neural cells. Peaks are colored by glycan subtypes and annotated with the schematic representations of the glycan structures. The GSL ceramide portions are denoted by the number of hydroxyl groups (d or t for di- or tri-hydroxy), total length of lipid, and the number of unsaturation. For example, d34:1 describes a ceramide with 2 hydroxyl groups, 34 total carbons, and 1 unsaturation. Glycan structures were drawn with GlycoWorkbench (Ceroni et al. 2008). Monosaccharide symbols follow the SNFG (Symbol Nomenclature for Glycans) system (Varki et al. 2015).

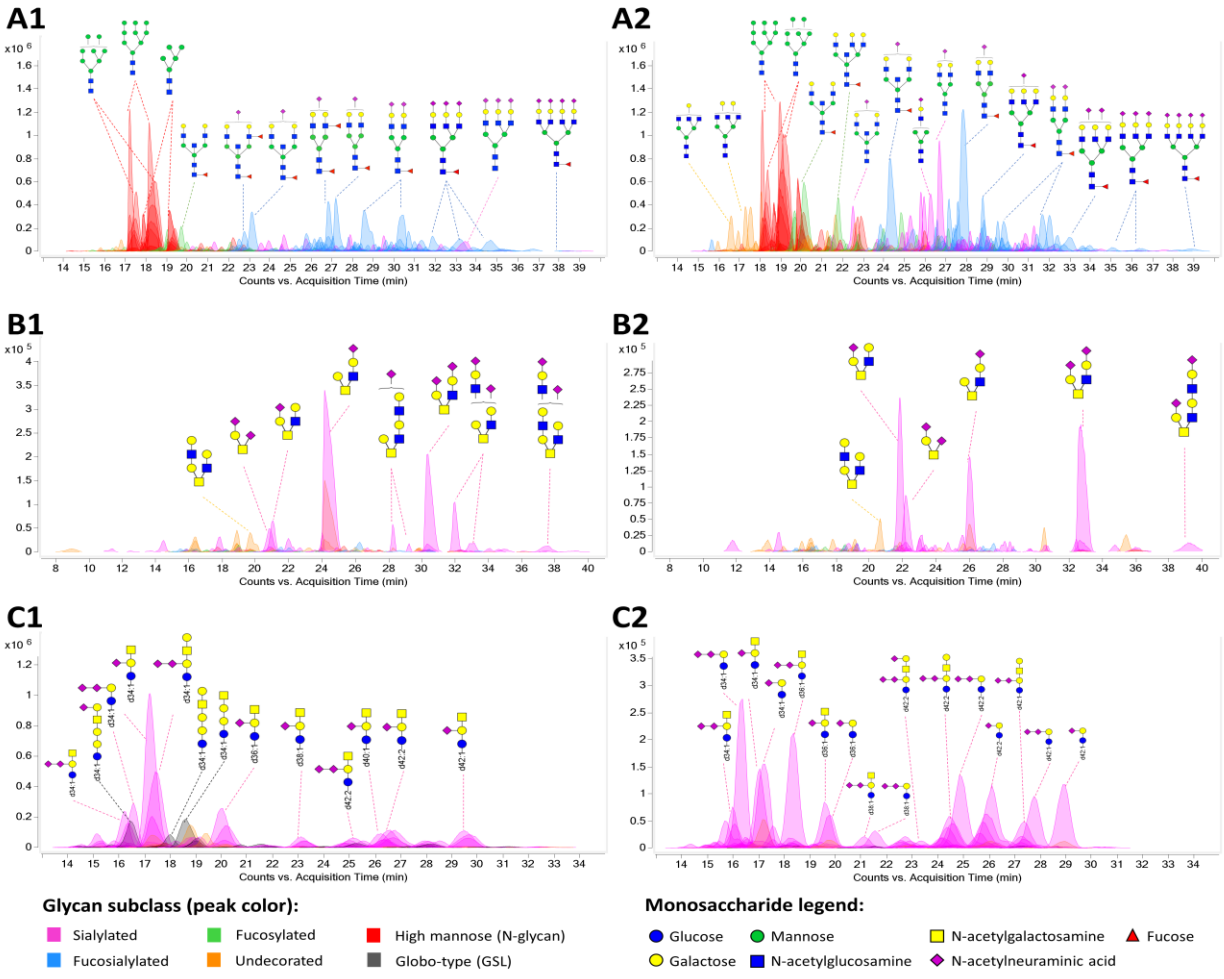

Figure 2: (A) Profile mass spectra of the $[M+2H]^{2+}$ ion of an N-glycan with composition $Hex_5HexNAc_4Fuc_1NeuAc_1$ from undifferentiated NTERA-2 cells. Because doubly charged species are shown, the mass shift due to ^{13}C labeling is 0.5 Da per labeled carbon. The mass spectra are corrected for the natural isotope distribution of carbon; the corresponding corrected isotopologue data are shown in the first column of (B). Corrected isotopologue data are also shown for the following representative glycans of each type of glycoconjugate: (B) N-glycan, $Hex_5HexNAc_4Fuc_1NeuAc_1$; (C) O-glycan, $Hex_2HexNAc_2NeuAc_1$; and (D) GSL, GM2(d34:1). Plots are shown for cells grown with regular glucose (ctrl) and [^{13}C-UL] monosaccharides (5 mM glucose, 5 mM galactose, 5 mM mannose, 5 mM fructose, and 100 uM fucose).

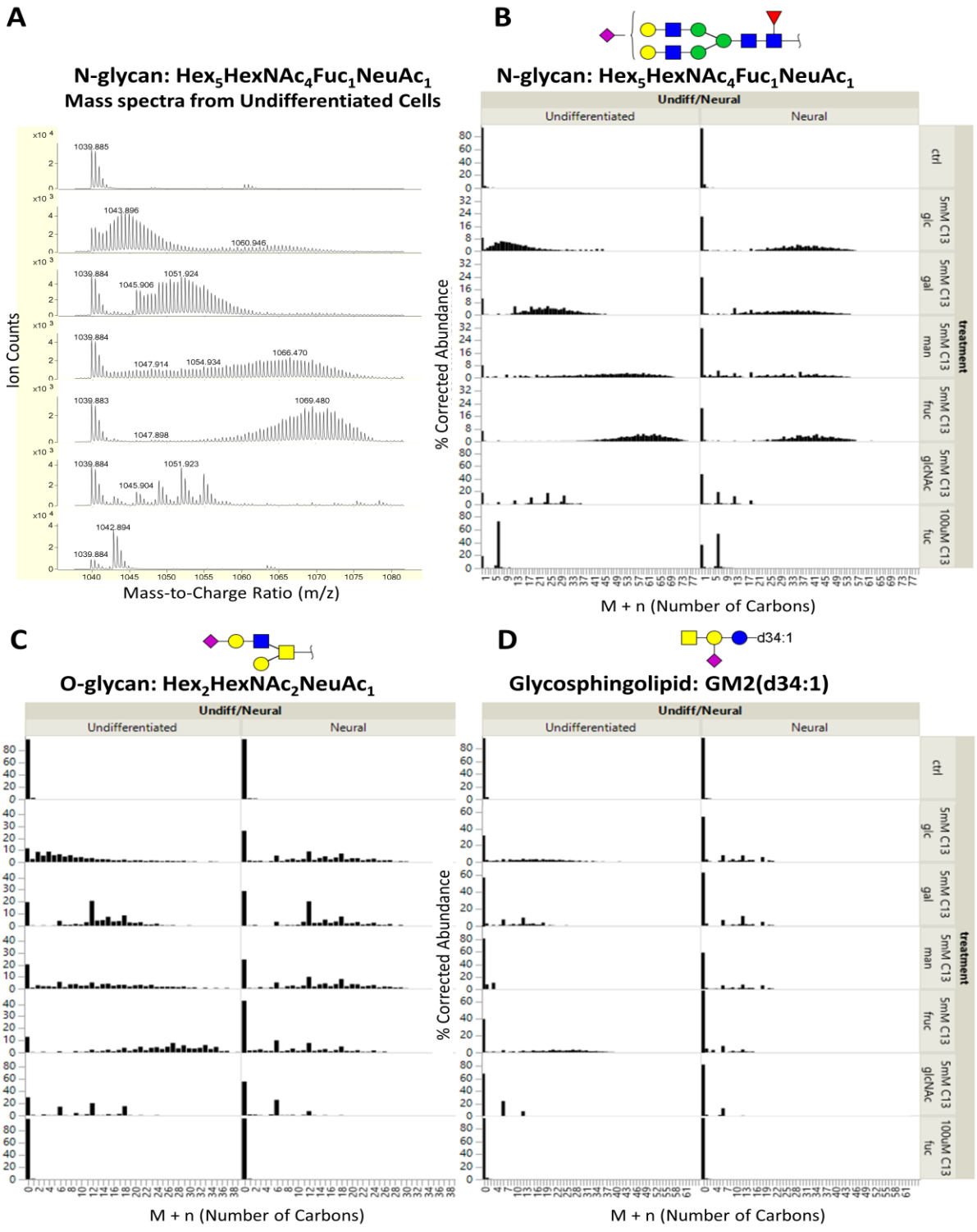

Figure 3: (A) Mean values for the extent of incorporation *%E* for N-glycans, O-glycans, and glycosphingolipids in both undifferentiated (blue) and neural (red) cells. The cells were fed with 5 mM of the indicated labeled monosaccharide for 72 h except for fucose, which was given 100 µM. Error bars indicate standard errors for identified glycans, with the N shown in blue text above each bar plot. Note that the GlcNAc values include only glycans with GlcNAc, GalNAc, and NeuAc, while fucose values include only fucosylated glycans because of the specificity of their incorporation. No fucosylated GSLs were detected. (B) Stacked bar plots showing the contribution of diffused incorporation *%Ed* (dotted pattern) and intact incorporation *%Ei* (solid pattern). Plots for individual glycan compositions are shown in **Supplementary Figure S2**.

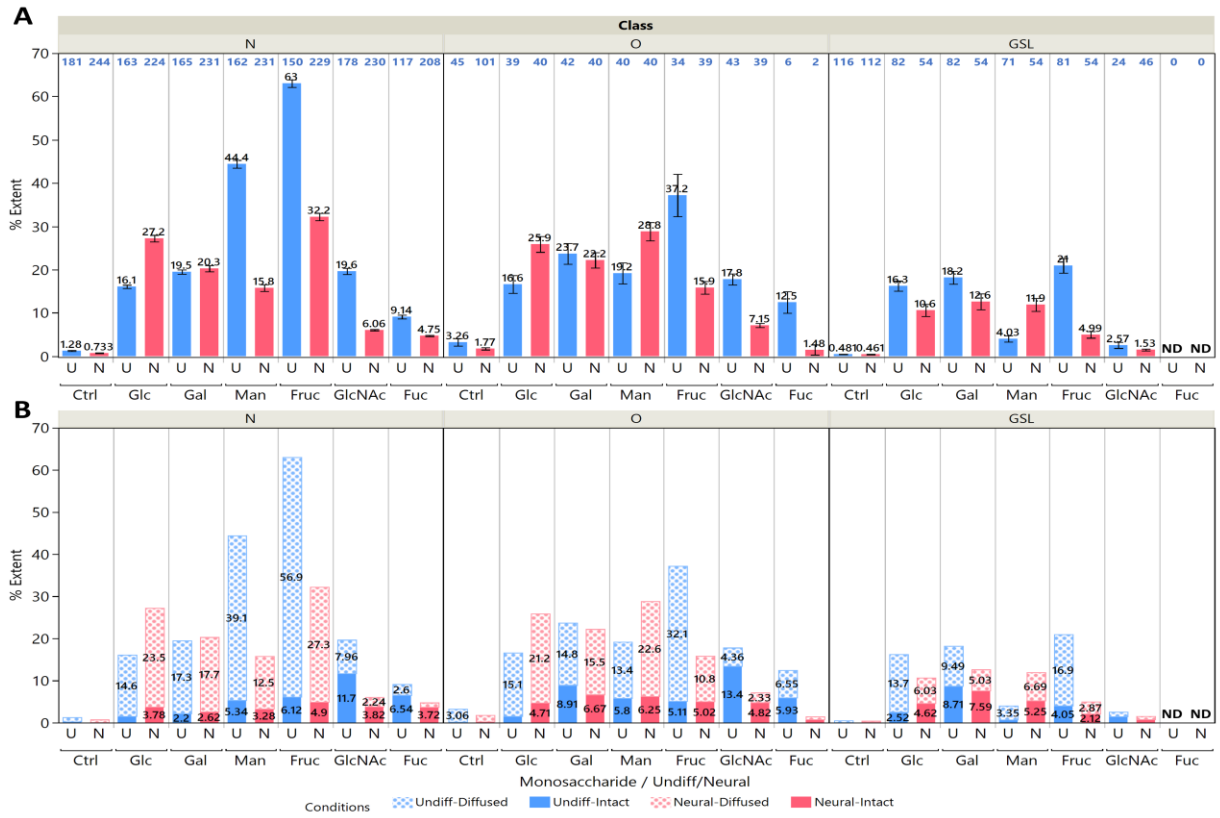

Figure 4: (A) Mean values for the extent of diffused incorporation *%Ed* and the extent of intact incorporation *%Ei* for N-glycans. Their sum represents the total extent of incorporation *%E*. Standard errors are shown for *N* ≈ 200 glycans. Plots for individual glycan compositions are shown in **Supplementary Figure S3**. (B) Isotopologue profiles for the bi-antennary complex N-glycan $Hex_5HexNAc_4Fuc_1NeuAc_1$ during co-feeding of 5mM [^{13}C-UL] galactose, mannose, or fructose with normal glucose at concentrations of 0, 0.10, 0.25, 0.50, 1.00, and 5.00 mM. Monosaccharide symbols are as follows: Mannose (green circle); Galactose (yellow circle); N-acetylneuraminic acid (NeuAc, pink diamond); N-acetylglucosamine (GlcNAc, blue square); Fucose (red triangle).

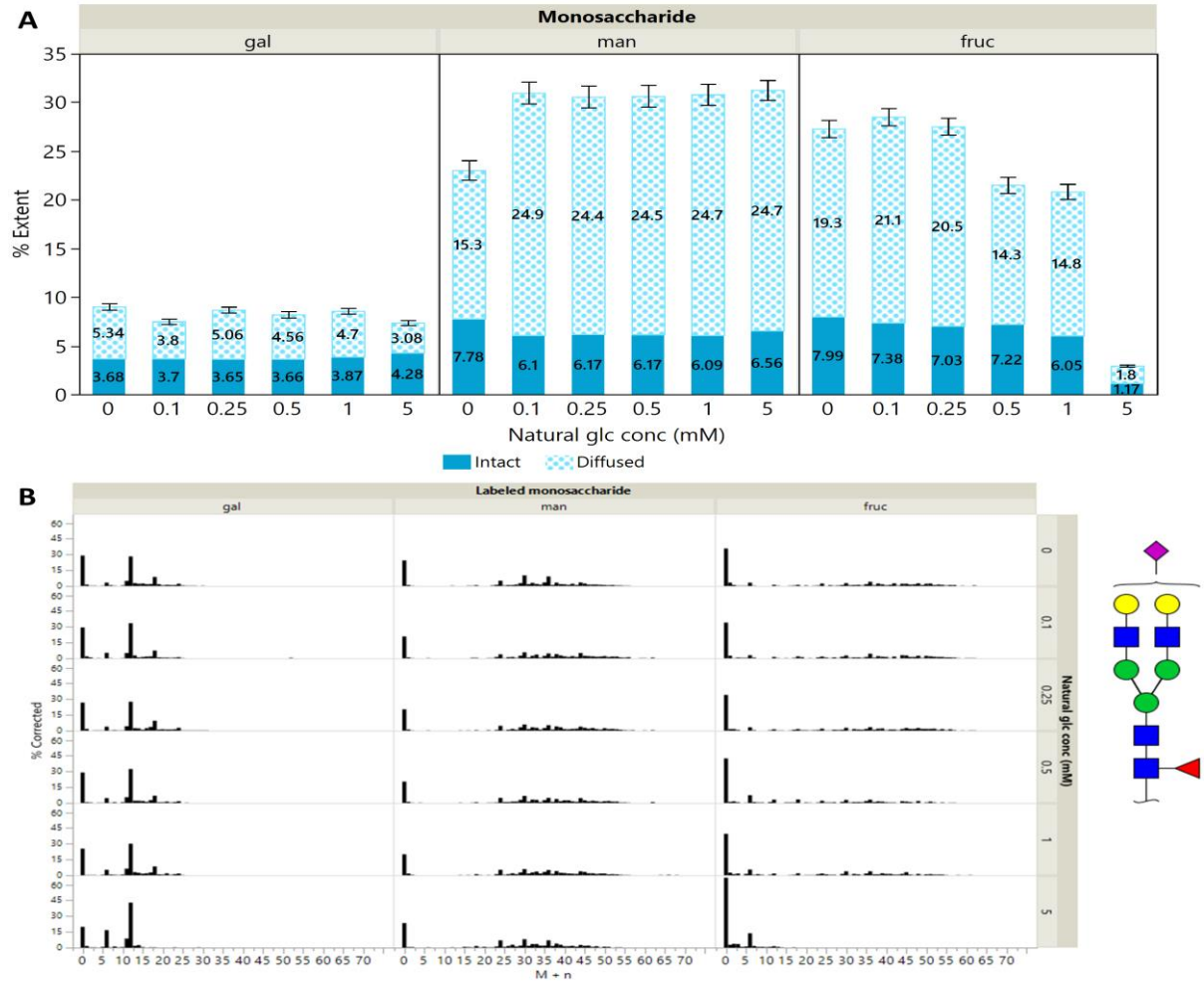

Figure 5: Mean values for the extent of diffused incorporation *%Ed* and the extent of intact incorporation *%Ei* for N-glycans, O-glycans, and GSLs. Standard errors are shown for the number of glycans listed in blue above each bar plot.

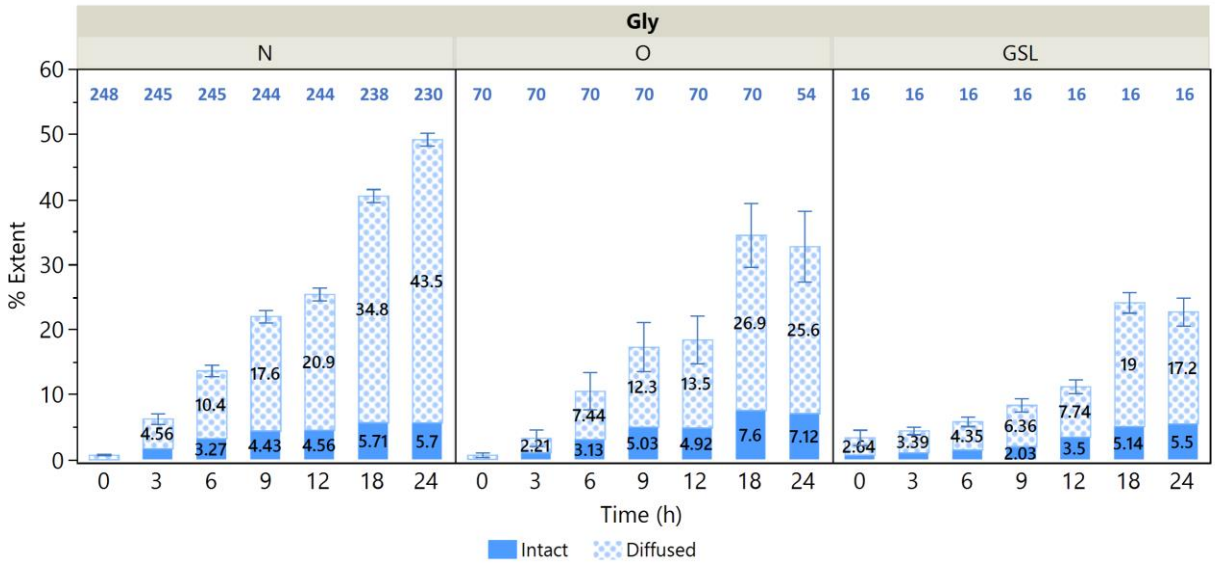

Figure 6: Incorporation curves showing the extent of incorporation *%E* plotted against time. (A) High-mannose type N-glycans (B) The mean *%E* of N-glycans grouped by subtype: C = complex, H = hybrid, C/H = complex/hybrid, HM = high-mannose. Error bars represent the standard error among the N-glycans of each subtype. N(C) = 95, N(C/H) = 76, N(H) = 29, N(HM) = 30. (C) Incorporation curves for triantennary complex-type N-glycans with 1-3 NeuAc and 0-1 Fuc. (D) Ganglioside GM2 with 32, 34, 36, and 42 ceramide carbons. N-Glycan composition legend: Hex_HexNAc_Fuc_NeuAc; GSL comp. legend: Hex_HexNAc_Fuc_NeuAc_NeuGc_Sulf_Ceramide lipid length_Degree of unsaturation.